DETECTION OF MOTION BLUR IN INTRATIVAL MICROSCOPY VIDEO IMAGES VIA ANALYSIS OF ORIENTED TEXTURE FEATURES

Carlos H. V. Pinto*, Bruno C. G. da Silva*, Danielle Bernardes**, Juliana C. Tavares**, Ricardo J. Ferrari*

* Department of Computer Science – Federal University of São Carlos, São Carlos (SP), Brazil
** Department of Physiology and Biophysics – Federal University of Minas Gerais, Belo Horizonte (MG), Brazil
e-mail: carlos.pinto@dc.ufscar.br

Abstract: *Intravital microscopy (IM) is an important experimental tool for the study of cellular and molecular mechanisms of leukocyte-endothelial interactions which occur in the microcirculation of various tissues and in various inflammatory conditions of in vivo specimens. Due to the limited control over the image acquisition conditions, the acquired video images can often have motion blur resulting mainly from the heartbeats and respiratory movements of the specimen. This problem can significantly undermine the results of both visual and computerized analysis over the IM videos. But since only a fraction of the total number of images is usually corrupted by severe motion blur, it is very important and desirable to have a procedure to automatically identify such images for posterior restoration. This work presents a new technique for the detection of motion blur in IM video images, based on directional (circular) statistics of local energy maps computed using a bank of 2D log-Gabor filters. In order to test the effectiveness of the proposed method, a quantitative assessment was conducted by testing each circular measure on 329 video images visually ranked by four observers. Results have shown areas under the ROC curves (AUC) of 0.95, outperforming the PSNR, SSIM and BIQAA metrics.*

Keywords: *detection of motion blur, in vivo image processing, blind image quality assessment, video processing.*

Introduction

Intravital microscopy (IM) is an imaging tool often used in quantitative and qualitative studies of leukocyte-endothelial cell interactions of *in vivo* specimens [1]. It allows a direct observation of leukocyte movements within microvessels of small animals under both normal and pathological conditions. In general, during the laboratory experiments, the leukocyte interactions are recorded as image sequences (videos), which are used for further visual analysis. Counting the numbers of rolling and adherent leukocytes and measuring the velocity of the rolling cells from IM video imagery are critical tasks in inflammation research and drug validation. However, due to the limited control over the image acquisition conditions, the acquired video images can often have motion blur resulting mainly from the heartbeats and respiratory movements of the specimen. This problem can significantly undermine the results of both visual and computerized analysis over IM videos. But since only a fraction of the total number of images in the video is usually corrupted by severe motion blur, it is necessary to have a procedure to automatically identify these images for posterior correction.

This work presents a new technique for automatic detection of motion blur in IM video images based on directional statistical analysis of 2D log-Gabor energy maps computed for different scales and orientations. Since log-Gabor are band limited filters, the computed energy measures are local in nature and add robustness to variations in illumination in the proposed analysis. This is an advantage since IM images may be degraded by the photobleaching effect [2] that may occur in the focal plane.

Materials and methods

Intravital microscopy – Female C57BL/6 mice were obtained from Animal Care Facilities of the Federal University of Minas Gerais (UFMG, Brazil). The Animal Ethics Committee of UFMG approved all experimental procedures used in this study. Intravital microscopy was performed on the mouse brain microvasculature as described in [1]. To assess the leukocyte-endothelium interactions, the fluorescent leukocytes were visualized under a Zeiss Imager M.2 (x20 long-distance objective lens; Göttingen, Germany) equipped with a fluorescent light source (epi-illumination at 510–560 nm, using a 590 nm emission filter). A video camera (Optronics) was mounted on the microscope in order to record images with a sampling rate of 16 frames/s, 8 bits depth and spatial resolution of 1.89 pixels/μm with a matrix size of 592×420 pixels.

Ground-truth image dataset – In order to quantitatively assess the results of the proposed method, an IM video composed of 329 frames was evaluated by a group of four observers without the presence of a reference image for comparison. It was used to form the ground-truth image data set. The observers were asked to give a rating score to each frame, according to their subjective judgment of image quality, considering both blurring and motion artifacts indiscriminately. The discrete rating system used to label the frames consisted

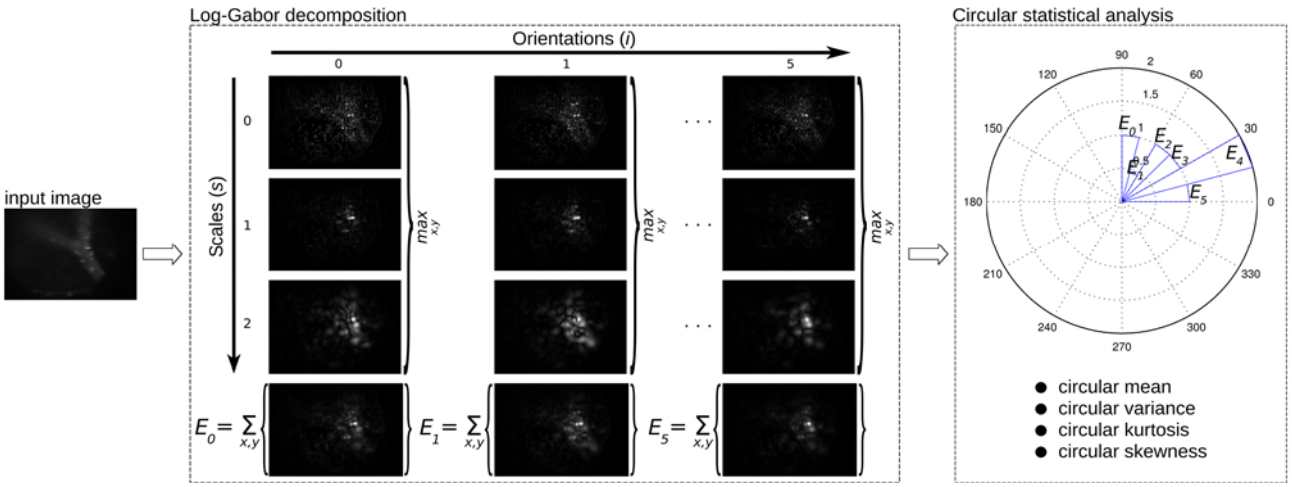

Figure 1: A schematic diagram to illustrate the main idea of the proposed method.

of integer numbers ranging from a low of 1 (bad quality) to a high of 5 (excellent quality). The final subjective score for each frame was assigned as the median of its individual ratings. Frames with score lower than or equal to two were labeled as visually bad for the purpose of quantitative analysis.

Method of evaluation – The performance of our technique was evaluated using receiver operating characteristics (ROC) curves [3] along with their respective areas (AUC – area under the ROC curve) with 95% confidence interval (CI). A single frame is considered a positive instance if it is labeled as "bad" (score ≤ 2) and a negative instance if it is labeled as "not bad" (score > 2).

Rationale of the proposed method – Each video frame is convolved with a bank of 2D log-Gabor filters to produce a set of local energy maps. By inspection of these maps, it was observed that, for a given set of scales (within a range of mid-spatial frequencies) and for different orientations, the maps present less variation on their energy distribution for a high-quality image when compared to the corresponding local energy maps of an image corrupted by motion blur. This can be explained by the fact that, in general, motion blur locally changes the image texture, introducing a great amount of directional information in the spectral bands that are not too low and not too high. Therefore, in order to capture such changes, the largest magnitude responses of the log-Gabor filters for a given orientation and across all scales are used in this work to build a resultant maximum energy image. The same procedure is applied for all orientations of the bank of filters and the resultant images are then assessed by using directional statistics and rose diagrams. A schematic diagram is shown in Figure 1 to illustrate the proposed approach.

The choice for log-Gabor filters is twofold: i) log-Gabor filters have zero DC component and therefore do not respond to regions with constant gray value intensities; ii) the transfer functions of the filters have extended tails covering high frequencies, thus making possible to obtain arbitrarily wide bandwidth, which can yield to a fairly uniform coverage of the frequency domain in an octave scale multiresolution scheme. In addition, the log-Gabor functions have been suggested to encode natural images more efficiently than the ordinary Gabor functions, which are frequently used in the literature for image filtering [4, 5]. Each 2D log-Gabor filter is constructed in the Fourier domain as a product of a radial and an angular component, as follows:

$$G(\omega,\theta)_{|\omega_s,\theta_i,\sigma_r,\sigma_\theta} = \\ = \exp\left(\frac{\left[\log\left(\omega/\omega_s\right)\right]^2}{2\sigma_r^2}\right)\cdot\exp\left(-\frac{(\theta-\theta_i)^2}{2\sigma_\theta^2}\right), \quad (1)$$

where ω_s is the central radial frequency of the filter for the scale s, σ_r is the logarithm of the scale bandwidth β, θ_i is the i_{th} orientation angle, and σ_θ is the angular standard deviation that determines the angular bandwidth of the filter.

For a given scale s and orientation i, the real valued transfer function of the 2D log-Gabor filter is convolved with the image and the results are extracted as simply the real component ($\Re_{i,s}$) for the even-symmetric filter and the imaginary component ($\Im_{i,s}$) for the odd-symmetric filter. Then, the oriented energy map $E_{i,s}$ is computed as follows:

$$E_{i,s}(x,y) = \sqrt{\left(\Re_{i,s}(x,y)\right)^2 + \left(\Im_{i,s}(x,y)\right)^2}. \quad (2)$$

In order to capture the texture changes introduced by motion blur, the following parameters were set for the design of the bank of filters: ω_{max} (maximum central frequency) $= \frac{1}{3}$ cycles/pixels, S (number of scales) = 3, β = 0.65 (i.e., frequency bandwidth σ_r approximately one octave), ω_{min} (minimum central frequency) = 0.075 cycles/pixels and σ_θ (angular standard deviation) = 1.2. The number of orientations was selected to allow a reasonable angular resolution in the representation of the energy distribution with minimum angular overlapping between the filters.

Directional (Circular) Statistics – After each image is decomposed into energy sub-bands using the bank of log-Gabor filters, a local energy map $E_i(x,y)$ is

obtained for each orientation i as the largest pixel-wise magnitude response of the log-Gabor filters across all scales. Then, for each E_i, the pixel values are accumulated as a real valued number (T_i) as follows:

$$T_i = \sum_{x,y} \max_{0 \le s < S} \{E_{i,s}(x,y)\}. \quad (3)$$

To compute the circular measures representing the angular dispersion of the magnitude responses of the log-Gabor filters, all T_i values were mapped to the range of $\left[0, \frac{\pi}{2}\right]$, producing the angular normalized values α_i. This procedure ensures the projections of the T_i vectors to the axes x and y will not cancel with one another. In this case, when the magnitude responses are similar (which is the expected case for high quality images) the angles α_i will be concentrated close to $\frac{\pi}{2}$ rads on unit circle. On the other hand, when an image is distorted by motion blur, the filters responses will be very different and, therefore, the angles α_i will be more uniformly distributed between 0 and $\frac{\pi}{2}$.

The following paragraphs describe the directional statistics used in this work and presented in [6].

The circular mean ($\bar{\alpha}$) is calculated as:

$$\bar{\alpha} = \tan^{-1}\left(\frac{\sum_{i=0}^{N-1} \sin(\alpha_i)}{\sum_{i=0}^{N-1} \cos(\alpha_i)}\right). \quad (4)$$

The magnitude of the mean resulting vector ($\bar{R}$) is closer to 1 as the data is more concentrated around $\bar{\alpha}$.

$$\bar{R} = \sqrt{(\sum_{i=0}^{N-1} \cos(\alpha_i))^2 + (\sum_{i=0}^{N-1} \sin(\alpha_i))^2} \quad (5)$$

The circular variance ($\bar{v}$) is closely related to $\bar{R}$ and is obtained as:

$$\bar{v} = 1 - \bar{R}/N \quad (6)$$

Notice that $\bar{v}$ will be always lower than 0.5 and it will be closer to zero for high quality images.

The circular kurtosis ($\bar{\gamma}$) is used as a measure of the distribution peakedness. It is calculated as:

$$\bar{\gamma} = \frac{1}{N}\sum_{i=0}^{N-1} \cos\big(2(\alpha_i - \bar{\alpha})\big) \quad (7)$$

Positive $\bar{\gamma}$ close to 1 indicates a strongly peaked distribution, and its value decreases when the distribution becomes flatter.

The skewness ($\bar{v}$) measures the lack of symmetry of a distribution. It is defined as:

$$\bar{v} = \frac{1}{N}\sum_{i=0}^{N-1} \sin\big(2(\alpha_i - \bar{\alpha})\big) \quad (8)$$

A $\bar{v}$ value close to zero is an indicative of a symmetric population around the mean direction. A negative value of $\bar{v}$ indicates that the data distribution is skewed left, and a positive value indicates that the distribution is skewed right.

Results

Figure 2 shows the distribution of all circular measures used in this work over the video images. Figure 3 presents the ROC curves, with their respective AUCs, obtained by the use of these circular measures for the detection of images affected by motion blur.

For the sake of comparison, the full-reference metrics PSNR and SSIM [7], as well as the blind metric BIQAA [8], were also tested for detection of the bad frames. Their resulting AUC values are presented in Table 1.

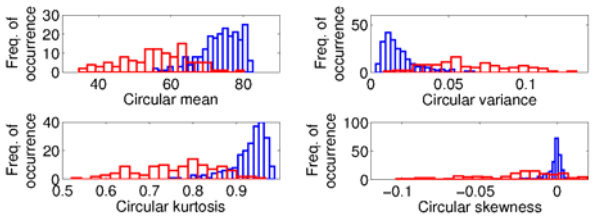

Figure 2: Distribution of all circular measures over the video frames. Blue: good frames. Red: bad frames.

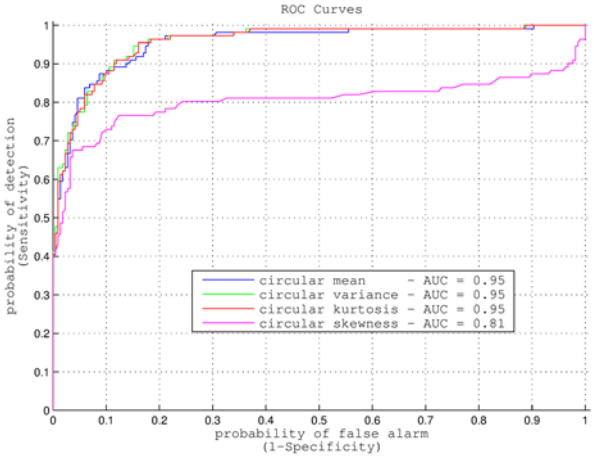

Figure 3: ROC curves for all circular measures used in this work, along with their respective AUCs.

Table 1: AUC values obtained with the full-reference metrics PSNR and SSIM and the blind metric BIQAA.

Metric name	AUC
PSNR	0.61
SSIM	0.73
BIQAA	0.74

Although real-time processing is not critical in this study, Table 2 presents the processing time of all algorithms used in this work to detect video motion blur.

Table 2: Processing time of all algorithms used to detect motion blur in 329 IM images.

Metric name	Processing time (min.)
Proposed method	8.2
PSNR	3.5
SSIM	4.0
BIQAA	9.4

All experiments were conducted using an Intel© Core™ i7 (3.33GHz) CPU machine (running Linux –

64–bit) with 24GB of RAM.

Discussion

Visual assessment of the plots in Figure 1 provides a strong indication that the circular mean, variance and kurtosis measures are, in fact, good candidates for detection of degraded frames. This was confirmed by the resulting AUC values, obtained individually for these measures. Our results show that circular variance values close to zero are associated to good quality images while bad frames present higher values. This is consistent with the definition of these measures, i.e., if all log-Gabor filters produce similar responses, then the circular mean will be concentrated on a one or few bins of the rose diagram and, therefore, the circular variance will be very small. However, if an image is degraded by motion blur, then the filter responses will be different for the orientations. The kurtosis measure has also shown very good results, which is also explained by the concentrated responses on a few bins of the rose diagram. For high quality frames, kurtosis values will be close to the unity.

Based on the AUC values and their respective 95% confidence intervals, we can conclude that there is no significant difference in the overall classification performance of the method using these features. The only feature that did not provide a very good performance was the circular skewness, which can be explained by differences in the video motion patterns that may pull the distribution tail to opposite directions.

By comparing our results with the data shown in Table 1, it can be observed that the proposed method outperforms the metrics PSNR, SSIM and BIQAA as a way for identifying images degraded by motion blur.

Conclusion

In this work we proposed a new method for the detection of motion blur in IM videos, which does not require any reference image and works on individual video images. Quantitative assessment of the proposed method using a real IM video composed of 329 frames have demonstrated its effectiveness; AUC values of 0.95 were obtained by using the proposed mean measure, circular variance and circular kurtosis. Our method outperformed the metrics PSNR, SSIM and BIQAA on the same task.

Acknowledgements

The authors are grateful to “Conselho Nacional de Desenvolvimento Científico e Tecnológico (CNPq)” – process number 481923/2010-1 – and to “Fundação de Amparo à Pesquisa do Estado de São Paulo (FAPESP)” – process number 2012/17772-3 – for their financial support during the course of this research.

References

[1] Santos AD, Roffe E, Arantes R, Juliano L, Pesquero JL Pesquero JB, Bader M, Teixeira M, Tavares JC. Kinin B2 receptor regulates chemokines CCL2 and CCL5 expression and modulates leukocyte recruitment and pathology in experimental autoimmune encephalomyelitis (EAE) in mice. Journal of Neuroinflammation. 2008; 5: 49-58.

[2] Viegas MS, Martins TC, Seco F, do Carmo A. An improved and cost-effective methodology for the reduction of autofluorescence in direct immunofluorescence studies on formalin-fixed paraffin-embedded tissues. European Journal of Histochemistry. 2007; 51 (1): 59-66.

[3] Fawcett T. An Introduction to ROC Analysis. Pattern Recognition Letters. 2006; 27 (8): 861-874.

[4] Field D. Relations between the statistics of natural images and the response properties of cortical cells. Journal of the Optical Society of America A. 1987; 4: 2379-2394.

[5] Kovesi P. Phase congruency: A low-level image invariant. Psychological Research. 2000; 64 (2): 136-148.

[6] Mardia KV, Jupp P. Directional Statistics. 1st ed. New York: John Wiley and Sons; 1999.

[7] Wang Z, Bovik A, Sheikh HR, Simoncelli E. Image Quality Assessment: From Error Visibility to Structural Similarity. IEEE Transactions on Image Processing. 2004; 13 (4): 600-612.

[8] Gabarda S, Cristóbal G. Blind image quality assessment through anisotropy. Journal of the Optical Society of America A. 2007; 24 (12): B42-B51.